

# Investigation of pH-Responsiveness inside Lipid Nanoparticles for Parenteral mRNA Application Using Small-Angle X-ray Scattering

Lukas Uebbing, Antje Ziller, Christian Siewert, Martin A. Schroer, Clement E. Blanchet, Dmitri I. Svergun, Srinivas Ramishetti, Dan Peer, Ugur Sahin, Heinrich Haas, and Peter Langguth\*



Cite This: *Langmuir* 2020, 36, 13331–13341



Read Online

ACCESS |



Metrics & More

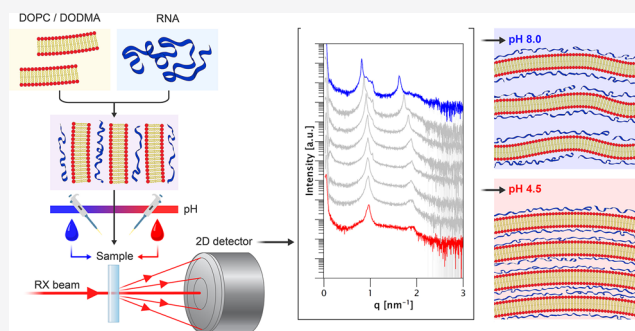


Article Recommendations



Supporting Information

**ABSTRACT:** Messenger ribonucleic acid (mRNA)-based nanomedicines have shown to be a promising new lead in a broad field of potential applications such as tumor immunotherapy. Of these nanomedicines, lipid-based mRNA nanoparticles comprising ionizable lipids are gaining increasing attention as versatile technologies for fine-tuning toward a given application, with proven potential for successful development up to clinical practice. Still, several hurdles have to be overcome to obtain a drug product that shows adequate mRNA delivery and clinical efficacy. In this study, pH-induced changes in internal molecular organization and overall physicochemical characteristics of lipoplexes comprising ionizable lipids were investigated using small-angle X-ray scattering and supplementary techniques. These changes were determined for different types of ionizable lipids, present at various molar fractions and N/P ratios inside the phospholipid membranes. The investigated systems showed a lamellar organization, allowing an accurate determination of pH-dependent structural changes. The differences in the pH responsiveness of the systems comprising different ionizable lipids and mRNA fractions could be clearly revealed from their structural evolution. Measurements of the degree of ionization and pH-dependent mRNA loading into the systems by fluorescence assays supported the findings from the structural investigation. Our approach allows for direct in situ determination of the structural response of the lipoplex systems to changes of the environmental pH similar to that observed for endosomal uptake. These data therefore provide valuable complementary information for understanding and fine-tuning of tailored mRNA delivery systems toward improved cellular uptake and endosomal processing.



In recent years, an upcoming new class of pharmaceutical drug products, messenger ribonucleic acid (mRNA)-based nanomedicines, has shown to be a promising alternative in a broad field of potential applications, ranging from protein substitution to tumor immunotherapy.<sup>1,2</sup> Research in this field has so far shown impressive results, reaching from basic research-related structural investigations, over proof-of-concept studies, all the way to clinical trials.<sup>3–9</sup> To provide a successful therapy in clinical practice, mRNA nanomedicines have to overcome several hurdles on their way to translation into proteins. The mRNA has to be protected from enzymatic degradation and delivered into its target cells, followed by cellular uptake, endosomal release, and finally expression of the protein.<sup>4,10,11</sup> The simple administration of pure mRNA does not fulfill this requirement, as it undergoes rapid degradation by nucleases, which are present ubiquitously in the human body. Therefore, the concept of using lipid-based nanoparticulate delivery systems for the mRNA has been introduced, and improved upon, throughout the years. Basically all of these approaches are based on the interaction of mRNA with cationic or ionizable lipids, resulting in complexation.<sup>12</sup> Prominent examples include lipoplexes based on synthetic cationic lipids, such as 1,2-di-*O*-octadecyl-3-

trimethylammonium propane (DOTMA) and 1,2-dioleoyl-3-trimethylammonium-propane (DOTAP), in combination with uncharged helper lipids, such as the phospholipids 1,2-dioleoyl-*sn*-glycero-3-phosphocholine (DOPC) and 1,2-dioleoyl-*sn*-glycero-3-phosphoethanolamine (DOPE), which have been studied structurally as well as tested for their therapeutic efficacy.<sup>3,4,7,13,14</sup> Other development has led to the synthesis of ionizable lipids, which are only positively charged at low pH, e.g., around pH 5.5, while at pH 7.4 they are charged to a lower amount or even completely uncharged.<sup>15</sup> Ionizable lipids are thought to be advantageous over their nonionizable homologous counterparts, as their pH-dependent charge can be used for reducing the toxicity effect of cationic lipids during systemic circulation while also facilitating a better release from the acidic endosome.<sup>16–18</sup> For these ionizable lipids (e.g.,

**Received:** August 18, 2020  
**Revised:** October 12, 2020  
**Published:** October 27, 2020





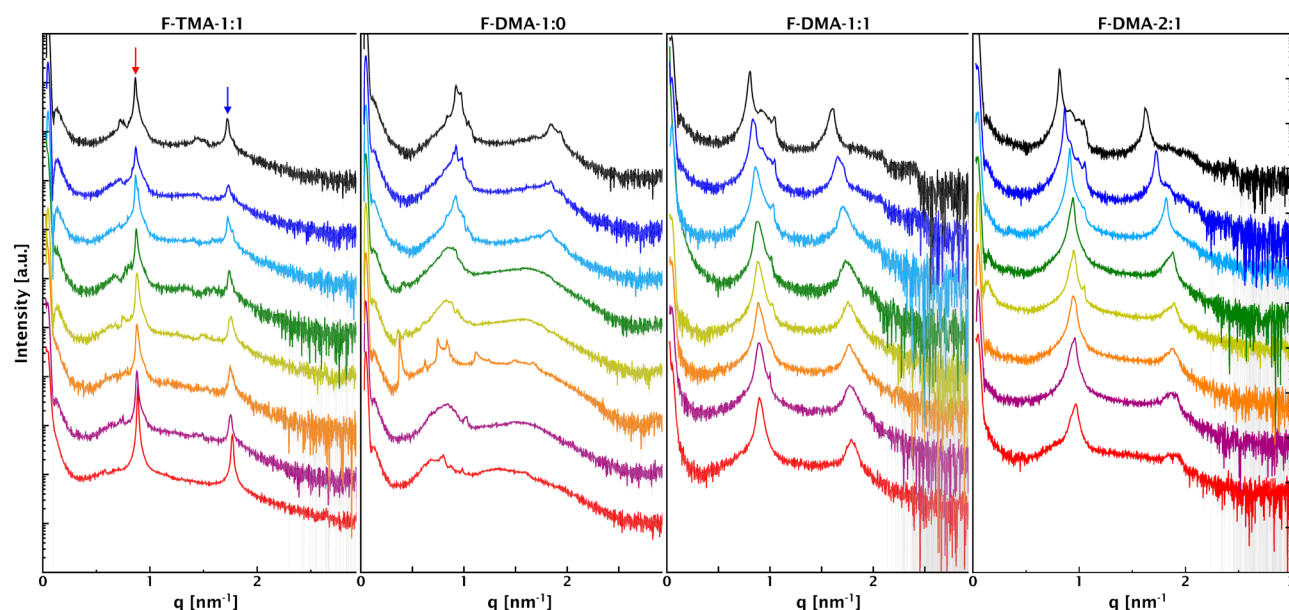


**Figure 2.** SAXS curves of samples containing DOTMA (TMA) or DODMA (DMA) at the N/P ratios indicated over a pH range of 4.5 (red curves, bottom) to 8.0 (black curves, top) in  $\Delta\text{pH} = 0.5$  steps. The N/P ratio of 1:0 indicates an mRNA-free sample. The intensities recorded at different pH values are displaced along the logarithmic axis for visualization. The patterns are in accordance with lamellar organization inside the membranes (integer peak spacing). In the scattering curves of F-TMA-1:0, the first and second orders of the main Bragg peaks are marked as red and blue arrows, respectively, representative of all scattering curves. While only subtle changes can be observed in the scattering curves of the preparation containing the permanently charged lipid DOTMA (F-TMA-1:1), pronounced structural changes can be observed for all samples containing the ionizable homologue DODMA.

structure with a lower population. In contrast, the scattering curves of all samples containing the ionizable lipid DODMA and mRNA showed a change in structure, where a clear shift of the main peak positions toward lower  $q$  (higher lamellar spacing, Figure 4) with increasing pH could be discerned. Additionally, secondary peaks evolved in the range of the strongest changes (between pH 6.5 and 7.0), potentially resulting from lateral phase separation into regions of higher and lower ratios of ionizable lipid and mRNA due to additionally present uncharged DODMA acting in a similar manner as the formally uncharged helper lipid DOPC, resulting in lower  $d$  spacing. The mentioned observed increase in  $d$  spacing with increasing pH, where the charge density and therefore also the repulsive electrostatic interactions inside the membranes decrease, might seem counterintuitive at first glance but can be explained by the fact that the negatively charged mRNA, sandwiched in between the lipid bilayers, acts like a “glue” and screens the charge of the lipid membranes. Upon decreasing the positive charge in the membranes by raising the pH, the negative charge contribution from the mRNA becomes more prominent and accounts for overall repulsive interactions between the bilayers.<sup>3</sup> It can be indirectly concluded that the mRNA remained immobilized in between the lipid bilayers for the whole pH range, even at pH 8.0. Quantitatively speaking, F-DMA-1:1 and F-DMA-2:1 showed lamellar order with  $d$  spacings of 70 and 65 Å, respectively, at pH 4.5, while at pH 8.0, this had shifted toward  $d$  spacings of 78 and 77 Å, respectively (see Table S1). Samples containing no mRNA (F-DMA-1:0) also showed pH responsiveness, but the changes in  $d$  spacing manifested in the opposite manner: At high pH values, when the lipids were uncharged, the formulation showed narrow lamellar peaks at relatively high  $q$ , therefore indicative of low  $d$  spacing. When lowering the pH and therefore increasing the charge of the lipids, these peaks

shifted to lower  $q$ , indicating an increase in  $d$  spacing, and became broader. In contrary to the situation for the mRNA-containing systems, here, in fact, the electrostatic repulsion between the equally charged lipid bilayers became effective with no mRNA to screen them, resulting in increased  $d$  spacing. The broadening of the peaks can be attributed to a loss of correlation perpendicular to the plane of the lipid bilayers, along with the increase of interbilayer spacing (see below and the Methods section for details). These observations are in line with results from previously measured samples consisting of DOPC and permanently charged lipids without mRNA.<sup>3</sup> There, the expected Bragg peaks from the multilamellar organization were measured for pure DOPC, while after the addition of cationic lipid, the resulting strong electrostatic repulsion between the charged cationic lipids induced a massive increase of  $d$  spacing and loss of correlation, resulting in a complete loss of visible peak structures in the regarded  $q$ -range. In the present study, the charge density resulting from the ionizable DODMA was continuously changed by variation of the pH. This pH variation therefore allowed for sensitive fine-tuning of the lamellar spacing and liquid crystalline order inside the multilayer stacks. Interestingly, under the conditions tested here, a complete loss of ordered structure was not observed. This can be taken as an indication that the charge density resulting from the ionizable lipids, even at low pH, is not as high as that from the permanently charged lipids, resulting in lower electrostatic repulsion and therefore a lower loss of correlation. As the structure was similar to that of pure DOPC multilayers at the highest tested pH level (8.0), it appears that the charge of the DODMA was too low to contribute effective electrostatic repulsion between the bilayers.<sup>26,27</sup>

The experiments described above showed that changes in the charge state of ionizable lipids as a function of pH result in

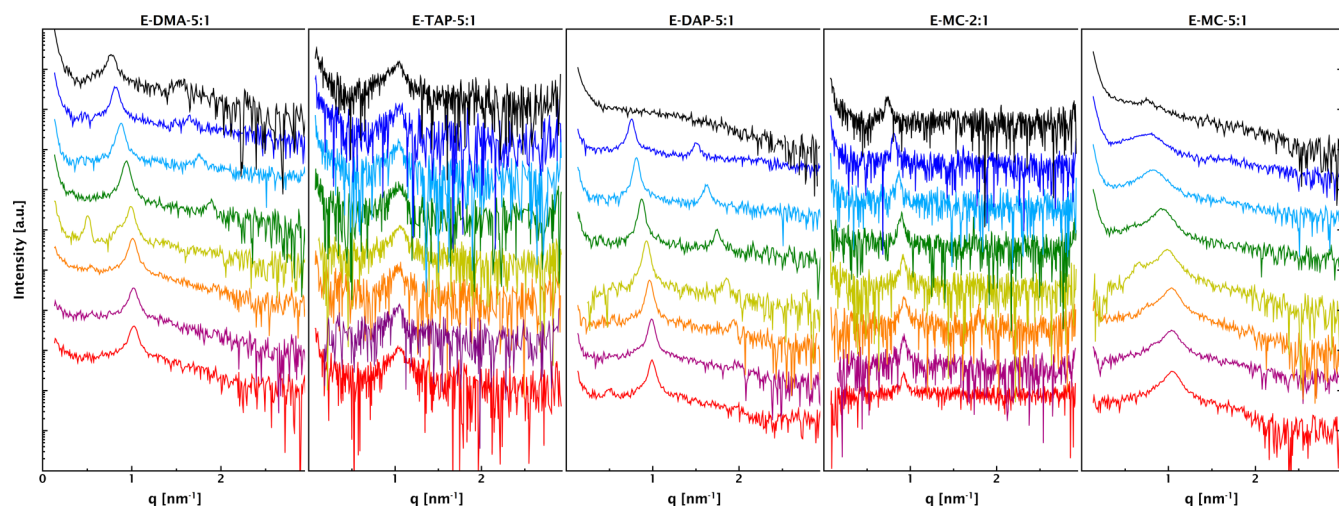


**Figure 3.** SAXS curves of samples prepared via the ethanol injection method over a pH range of 4.5 (red curves, bottom) to 8.0 (black curves, top) in  $\Delta\text{pH} = 0.5$  steps. The intensities recorded at different pH values are displaced along the logarithmic axis for visualization. Additionally to DOPC, the systems comprised DODMA (DMA), DOTAP (TAP), DODAP (DAP), or DLin-MC3-DMA (MC) and mRNA at the N/P ratios indicated. The difference in noise level is due to different experimental setups (sample–detector distance) and does not indicate a difference in sample quality.

distinct effects on the molecular organization inside the lipoplex systems, which can be sensitively determined by SAXS. Qualitatively, the effects were very similar with different fractions of the ionizable lipid inside the membrane, with the quantitative effects becoming more pronounced at higher fractions. The subsequent SAXS experiments were therefore performed with a higher fraction of the ionizable lipid in the membrane, while the mRNA fraction was kept constant, leading to higher N/P ratios.

As this second line of experiments was performed at an instrument with a significantly lower photon flux and the samples were prepared with a different technique (ethanol injection; for reasoning, see [Sample Nomenclature, Formulation, and Laboratory Physicochemical Characterization](#)), which only works at lower sample concentrations than the lipid film method, the measured intensities were noisier than those for the first line of experiments, as can be seen by comparing [Figures 2 and 3](#). This, however, does not impact the interpretation performed in this study, since no intensity-related information (e.g., peak area, area under the curve) was interpreted. Therefore, the data are comparable in the context of this study. In addition to DODMA, the structurally similar counterpart DODAP and its permanently charged homologue DOTAP, as well as the ionizable lipid DLin-MC3-DMA, were used for the preparation of lipoplex systems. DLin-MC3-DMA is considered to have improved transfection efficacy due to its optimized  $\text{pK}_a$  value and is part of the Food and Drug Administration (FDA)- approved siRNA lipid nanoparticle product Onpattro (Alnylam Pharmaceuticals).<sup>24</sup>

As expected, the scattering curves for E-DMA-5:1 showed the same trends as for the previous DODMA-containing samples but to an even higher degree ([Figure 3](#)). Again, the main peak shifted to lower  $q$ -values when raising the pH, corresponding to an increase in  $d$  spacing from 61 to 81 Å ([Figure 4](#) and [Table S1](#)). Combining this  $\Delta d$  of about 19 Å with the above-mentioned results for F-DMA-1:1 and F-DMA-2:1, one can see that this connotes a monotonously increasing relationship between the molar fraction of DODMA and the maximum pH-dependent change in  $d$  spacing (see [Figure S4](#)). Again, samples containing permanently charged lipids (E-TAP-

5:1) showed a lamellar structure with no structural changes or trends over the measured pH range ([Figure 4](#)) and with a  $d$  spacing of 60–61 Å. Preparations containing the ionizable homologue DODAP (E-DAP-5:1) on the other hand showed a clear shift of the main Bragg peak toward lower  $q$ -values with rising pH, corresponding to an increase of  $d$  spacing from 63 to 83 Å (at pH 7.5), and a complete and abrupt loss of structure was observed at pH 8.0. Formulations containing DLin-MC3-DMA were prepared at N/P ratios of 2 (E-MC-2:1) and 5 (E-MC-5:1). E-MC-5:1 showed broader Bragg peaks in comparison to the DODMA and DODAP systems, but the shift of peak positions was clearly discernible for both formulations, with the calculated  $d$  spacing shifting from 68 to 85 Å and from 60 to 81 Å, respectively. Additionally to the shifted position of the main Bragg peak, E-MC-5:1 also showed a gradual change of peak width. Similar to the observations with the mRNA-free systems comprising ionizable lipids, it appears that the positional order decreased with the changing charge state in this case as well. The Bragg peak made out at pH 4.5 shifted toward a broader, more asymmetrical, and less defined peak, until finally at pH 8.0, barely any peak could be made out at all. Interestingly, such observations pointing toward a gradual loss of positional order were not made for the other ionizable lipids, DODMA and DODAP, in the pH range observed here. Only for E-DAP-5:1 at pH 8.0, the already mentioned abrupt loss of structure occurred.

For further data analysis, the  $d$  spacings were plotted against the pH value ([Figure 4](#)). As can be seen, the values for the systems comprising ionizable lipids changed in a sigmoidal manner, allowing sigmoidal (Boltzmann) fitting. For E-MC-2:1, the measured peak position for pH 8.0 was not included in the fitting range, as including it in the fitting process produced nonsensical results. From the fits, inflection points, which were interpreted as the “conformational transition points” of the systems (similar to the  $\text{pK}_a$  of a molecule but describing the conformational change of the delivery system as a whole, instead of the charge ratio of the ionizable lipid), were determined (see [Table 1](#)). In these diagrams, the already observed contrary trends of systems comprising only the ionizable lipids, but no mRNA (decrease of  $d$  spacing with

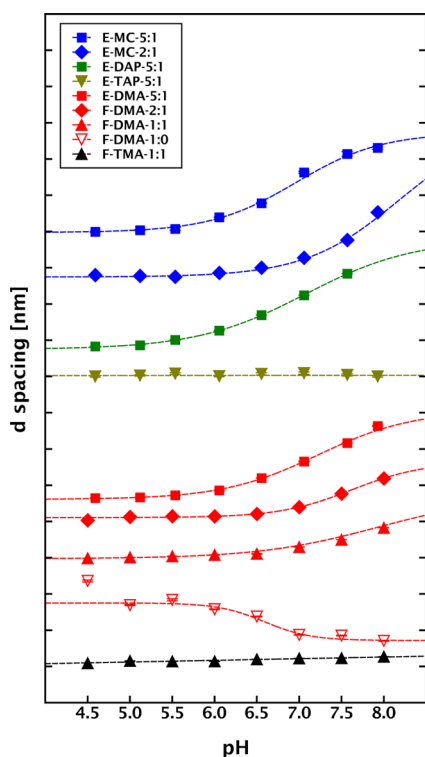


**Figure 4.**  $d$  spacing calculated from the peak position of the first maximum for all formulations measured via SAXS. Sigmoidal (Boltzmann) fits (dashed lines) were calculated using QtiPlot, where applicable. Error bars represent the (propagated) errors from the peak fitting process. Curves are shifted vertically for visual clarity on a relative scale (tick marks indicative of 1 nm), while the absolute numbers can be found in Table S1. The lowest trace (black) shows the lipoplexes based on the permanently charged lipid DOTMA, which shows no significant pH-dependent changes, with the results for systems comprising DOPC and DODMA, but no mRNA, just above (inverse red triangles). On top are the lipoplex systems comprising mRNA and the permanently charged lipid DOTAP (dark yellow inverse triangles), and those comprising the ionizable lipids DODMA, DODAP, and DLin-MC3-DMA, with the N/P ratios as indicated.

increasing pH), and those with mRNA (increase of  $d$  spacing with increasing pH) are obvious. In addition, the increase of total change in  $d$  spacing with increasing fraction of ionizable lipids is clearly discernible. Furthermore, the analysis of the conformational transition points as a function of mRNA and ionizable lipid fraction (N/P ratio) allows additional insight into the systems. With increasing amounts of mRNA in relation to the ionizable lipid, the conformational transition points shift monotonously to higher values, as can be most clearly seen in Figure 5, for the example of DODMA comprising systems. Thus, the data indicate that the conformational transition points can be affected not only by the selection of the ionizable lipid but also by the selection of the N/P ratio. Therefore, with the N/P ratio variation, an additional and sensitive method for accurate tuning of the conformational transition points is given.

Furthermore, the peak widths of the different samples were determined, which correlate with the positional order inside the organized stacks, with an increase of peak width being the result of a decrease of positional order. Taking into account a frequently used formalism for liquid crystalline order, the

**Table 1.** Comparison of Conformational Transition Point and Apparent  $pK_a$  Values Calculated from Sigmoidal (Boltzmann) Fits of Either the Scattering Vector  $q$  of the Main (First Order) Bragg Peaks or the TNS-Assay Intensity for Each Formulation<sup>a</sup>

cationic lipid	N/P ratio	conformational transition point from SAXS	apparent $pK_a$ from TNS
DOTMA	1:1	n.c.	—
	5:1	n.c.	n.c.
DODMA	no mRNA	$6.6 \pm 0.2$	$7.1 \pm 0.2$
	1:2	—	$7.9 \pm 0.1$
	1:1	$7.7 \pm 0.1$	$8.0 \pm 0.0$
	2:1	$7.5 \pm 0.1$	$7.6 \pm 0.0$
	5:1	$7.0 \pm 0.1$	$7.2 \pm 0.1$
DOTAP	5:1	n.c.	n.c.
DODAP	no mRNA	—	$7.3 \pm 0.1$
	2:1	—	$7.5 \pm 0.1$
	5:1	$6.8 \pm 0.1$	$7.8 \pm 0.2$
DLin-MC3-DMA	no mRNA	—	$7.4 \pm 0.2$
	2:1	$7.4 \pm 0.5$	$7.7 \pm 0.3$
	5:1	$6.8 \pm 0.1$	$7.3 \pm 0.1$

<sup>a</sup>Formulations not measured with the respective method are marked with “—”, and measurements where no meaningful Boltzmann fit could be applied are marked with “n.c.” (not calculated).

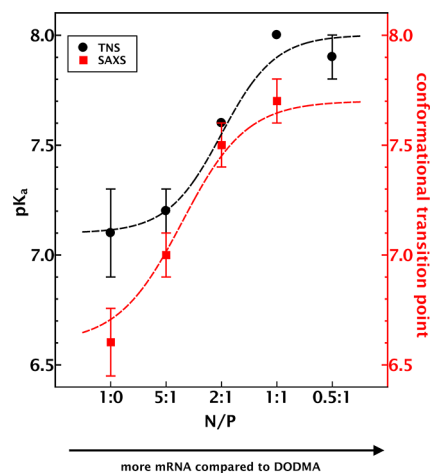


**Figure 5.** Comparison of the formulations' conformational transition point and lipid  $pK_a$  for samples comprising the ionizable lipid DODMA as determined by SAXS (red) and TNS (black). Dashed lines are meant as a guide to the eye and do not represent fitting of a physical model.

correlation length is given as  $2/\Delta q$  (scaling inversely with the peak width  $\Delta q$ , see the Methods section for details).<sup>28</sup>

While for most samples the peak width did not significantly change over the whole pH range, E-MC-5:1 showed an obvious trend to broader peaks, and therefore decay of positional order, with increasing pH (Figure 6).<sup>28</sup> On the contrary, the mRNA-free system F-DMA-1:0 showed the opposite effect, as there was an increase of positional order with increasing pH. Interestingly, such observations pointing toward a loss of positional order were not that obvious for the other ionizable lipids DODMA and DODAP. Only with DODAP (E-DAP-5:1), which showed clear and defined Bragg peaks over the whole pH range, an abrupt loss of lamellar structure at pH 8 was observed. This more pronounced effect of DLin-MC3-DMA on the organization of the lipoplex

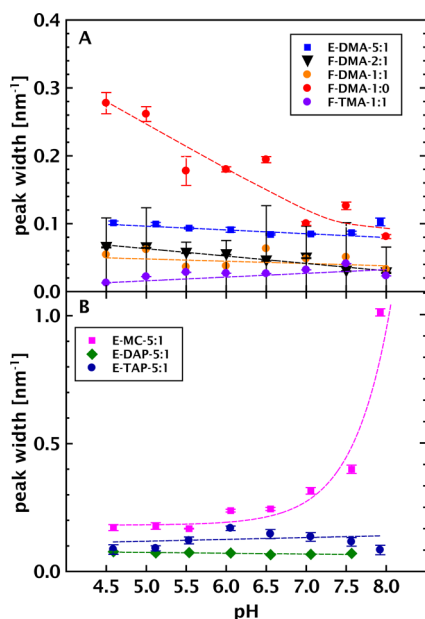


**Figure 6.** Peak width vs pH for the main Bragg peak for samples measured by SAXS, as determined from Lorentz fit analysis. Error bars represent the propagated errors from the peak fitting process. Dashed lines are meant as a guide to the eye and do not represent fitting of a physical model. (A) Samples comprising DODMA or DOTMA. (B) Other samples with an N/P of 5:1.

clusters may be related to its overall lower  $pK_a$  value in comparison to the other two ionizable lipids. Combining this observation with its lower  $pK_a$  value, this may contribute to the high transfection efficacy of DLin-MC3-DMA formulations in certain settings, particularly for hepatic targeting.<sup>21,29</sup>

**$pK_a$  Fluorescence Assays.** For comparison, the systems were investigated by a frequently used fluorescence assay, which utilizes the fluorescent dye TNS to measure the lipid  $pK_a$ . As expected, this assay also showed clear sigmoidal behavior for all formulations based on ionizable lipids (Figure S5), while no such changes could be observed for formulations based on permanently charged cationic lipids. Sigmoidal (Boltzmann) fits were applied to the experimental data here as well, and the inflection points were defined as the apparent  $pK_a$  of these formulations (see Table 1 and Figure S5).

Looking at the results from the TNS assay, one can see that the results were qualitatively similar and showed the same trends as the SAXS data. Notably, the molar ratio of ionizable lipid influenced the pH responsiveness of the lipoplexes here as well. As was the case for the change in  $d$  spacing, the difference in fluorescence intensity between the lowest and highest pH increased with higher N/P ratios, while samples containing no mRNA showed an even greater intensity shift than samples containing the same amount of ionizable lipid but with mRNA. Both of these results can be explained by the mechanism of action behind the assay.<sup>30</sup> Since TNS can only show fluorescence if it is bound to cationically charged lipids, higher fractions of ionizable lipids result in higher fluorescence intensities for constant TNS concentrations, as long as there is an excess of TNS. As the mRNA competes for electrostatic binding sites with TNS, its absence leads to higher concentrations of lipid-bound TNS and therefore higher maximum intensities.

## DISCUSSION

It is a widely accepted paradigm that the transfection efficacy of RNA lipid nanoparticles sensitively depends on the  $pK_a$  value of the ionizable lipid used for particle formation. In particular, the increasing charge on lowering the pH is considered important for endosomal processing and release. Various mechanisms including facilitated phase transitions (e.g., toward the inverse hexagonal phase) or elevated electrostatic membrane interactions at the lower pH levels in the endosomal compartment are believed to play a role in these processes.<sup>21</sup> However, clear insight and understanding of these factors and coherencies are still pending. The standard technique to investigate pH responsiveness in lipid nanoparticles utilizes the fluorescence readout of a lipid-binding dye. This gives information on the charge state of the ionizable lipids accessible to the dye, but information on the overall conformation of the lipoplexes can only be derived from this assay indirectly. Here, we have directly investigated the pH-dependent structural features inside mRNA lipoplex model systems comprising ionizable lipids.

The SAXS measurements performed in this study provided an accurate measure of the structural reorganizations as a function of pH in lamellar model lipoplex systems comprising ionizable lipids and mRNA. Most prominent were pronounced changes in the repeat distances inside the lipoplexes, which allowed us to determine the conformational transition point of the overall lipoplex assemblies. Changes of the correlation length and/or increase of the  $d$  spacing and emergence of patterns with different characteristic spacing provided complementary indications on the influence of pH changes on the molecular organization inside the lipoplex stacks. While the results correlated with observations from the established TNS technique, they allowed to get further, refined insight into the structural changes induced by pH variations. The observations could be convincingly explained by the modulation of protonation of the ionizable lipids on the pH variation. Due to fading protonation upon increasing pH levels, the attractive forces between the lipid membrane and mRNA decrease, leading to elevated distances between the bilayers, i.e., higher  $d$  spacing and lower correlation between the lipid stacks. The effect of changing protonation of the ionizable lipid was also verified by the observations from measurements without the mRNA inserted in between the lipid bilayers, where the pH variation had the opposite effect, namely, a decrease of  $d$  spacing and increase of correlation with increasing pH. Notably, although the SAXS measurements showed less dense packing for systems comprising mRNA at high pH, the mRNA was not released from the multilayer stacks as indicated by both the gel electrophoresis and the RiboGreen assay (an illustration of this process can be seen in the article abstract). These results indicate that the stability in circulation might be maintained.

When comparing the pH-dependent structural changes observed in the SAXS measurements to the findings gained from the TNS assay the calculated  $pK_a$  values showed a systematic shift to higher values for the fluorescence assay, with a maximum discrepancy of about 1.2 between the apparent formulation  $pK_a$  and the conformational transition point of E-MC-2:1. This observation may be helpful for the correct interpretation of membrane occurrences, such as those involved in endosomal processing, at the molecular level. It appears plausible that the structural changes depend not only

on the protonation state of the ionizable lipid, but rather the overall lipid assembly has to be taken into account. As further notable information in this context, both SAXS and TNS measurements indicated that the conformational transition point also depended on the fraction of the mRNA inside the membranes, where a monotonous change over about 1 pH value as a function of the N/P ratio was determined. Thus, the conformational transition points seem to be dependent on three factors: the type of the ionizable lipid, its molar fraction within the particles, and the ratio of the ionizable lipid to the mRNA (known as the N/P ratio). Comparing formulations with the same molar ratios of ionizable lipid, those containing DODMA showed the highest conformational transition point, followed by DODAP-containing formulations, while DLin-MC3-DMA-containing lipoplexes showed the lowest conformational transition points of the tested systems.

In addition to their  $pK_a$ , the fusogenicity of different lipids, which results from their ability to form the reversed hexagonal phase  $H_{II}$ , has an influence in facilitating endosomal escape.<sup>30</sup> Both of these lipid properties, which are a result of both the headgroup structure and lipid tail saturation, are therefore important factors to be kept in mind when choosing lipids for mRNA lipoplex formulation. While the conformational transition point of the formulation can only be controlled by the choice of the ionizable lipid and its molar fraction within the lipoplex, fusogenicity can also be improved by utilizing helper lipids such as DOPE, which is known to show a tendency for forming an inverse hexagonal phase  $H_{II}$ .<sup>31</sup> Recently, certain further structural aspects, correlated to the degree of order and the microdomain structure inside the particles, have also proven to be favorable for transfection efficacy. So-called lipid nanoparticles (LNPs), which utilize cholesterol and PEG-functionalized lipids in addition to high fractions of ionizable lipids and helper lipids, as well as hybrid systems, utilizing both charged lipids and charged polymers, have shown strong transfection rates in vitro and in vivo when ordered domains and regions of low order coexisted.<sup>32</sup> These LNPs and hybrid systems, combined with the understandings gained from this study, can prove to be the next big step in utilizing lipid-based mRNA delivery systems for cancer immunotherapy, as they offer the possibility of stealth and targeting functionalization to specifically and efficiently target specific subpopulations of immune cells, such as dendritic cells or T cells, and therefore improve clinical efficacy.

Overall, the results from this study provide a contribution for a better understanding of the structural and functional coherencies inside mRNA nanoparticles comprising ionizable lipids. Such understanding may help to assemble mRNA delivery systems with fine-tuned responsiveness to changes of pH in the local environment to obtain optimized expression in a given target.

## CONCLUSIONS

With the measurements reported here, improved and accurate insights into the pH-dependent structural organization in lipidic mRNA delivery systems comprising ionizable lipids were obtained. The most obvious observations could be made based on the SAXS measurements, where pronounced changes in the scattering patterns were determined. The applied model systems allowed us to accurately determine changes of  $d$  spacing as a function of pH, which correlated well with observations from established techniques such as the TNS fluorescence assay. Options to precisely modulate pH

responsiveness beyond chemical modification of the ionizable lipid were outlined. These results will help with the further fine-tuning of formulations to improve the activity of mRNA nanomedicines for a given target cell population.

## MATERIALS

Synthetic mRNA, which was provided by BioNTech SE (Mainz, Germany), was synthesized using internal protocols as published earlier (R159 consisted of ~1670 nucleotides, while R18 consisted of ~1900 nucleotides).<sup>33</sup> Noncoding mRNA was used for all characterization steps. 1,2-Dioleoyl-*sn*-glycero-3-phosphocholine (DOPC), 1,2-dioleoyl-3-trimethylammonium-propane (chloride salt, DOTAP), 1,2-dioleoyl-3-dimethylammonium-propane (DODAP), 1,2-dioleoyloxy-3-dimethylaminopropane (DODMA), and 1,2-di-*O*-octadecenyl-3-trimethylammonium propane (chloride salt, DOTMA) were purchased from Avanti Polar Lipids (Alabaster, AL). (6Z,9Z,28Z,31Z)-Heptatriacont-6,9,28,31-tetraene-19-yl 4-(dimethylamino)butanoate (DLin-MC3-DMA) was synthesized by the lab of Prof. Dan Peer (Tel Aviv, Israel). Ampuwa was obtained from Fresenius Kabi Deutschland GmbH (Bad Homburg vor der Höhe, Germany), and chloroform and RNaseZap were purchased from Sigma-Aldrich (St. Louis, MO). Nuclease-free water, ethylenediaminetetraacetic acid (EDTA), *N*-(2-hydroxyethyl)piperazine-*N'*-ethanesulfonic acid (HEPES), and glycylglycine (GG) were purchased from Carl Roth (Karlsruhe, Germany). Absolute ethanol (200 proof) and Dulbecco's phosphate-buffered saline (DPBS) were purchased from Fisher Scientific (Schwerte, Germany). For the sample preparation via the ethanol injection method, SOFT-JECT syringes from Henke-Sass, Wolf (Tuttlingen, Germany) and 27G Sterican needles (B. Braun Melsungen AG, Melsungen, Germany) were used.

For the  $pK_a$  fluorescence assay, 6-(*p*-toluidino)-2-naphthalenesulfonic acid sodium salt (TNS), potassium dihydrogen phosphate, and disodium hydrogen phosphate were purchased from Sigma-Aldrich (St. Louis, MO), while dimethyl sulfoxide (DMSO) was purchased from VWR International GmbH (Darmstadt, Germany). RiboGreen RNA reagent for the determination of accessible mRNA was obtained from Fisher Scientific (Schwerte, Germany). For the determination of free mRNA, agarose was obtained from Biozym (Hessisch Oldendorf, Germany), and 10× Tris-borate-EDTA (TBE) buffer from Carl Roth (Karlsruhe, Germany) and Gel-Red nucleic acid gel stain from Biotium (Fremont, CA) were used for the preparation.

## METHODS

**Nuclease-Free Working.** To ensure a nuclease-free environment, glassware was exposed to temperatures of  $\geq 300$  °C for at least 12 h and nuclease-free disposable equipment was used where possible. All other equipment was treated with RNaseZap prior to use.

**Lipoplex Preparation.** Lipoplexes were prepared using two different methods. For samples prepared via the lipid film method, the lipids were dissolved in chloroform, mixed in the required ratios, and pipetted into a glass vial. The chloroform was evaporated using rotary evaporation on a Büchi Rotavapor (BÜCHI Labortechnik GmbH, Essen, Germany), creating a thin lipid film. The films were then stored at  $-25$  °C for at least 12 h. The mRNA was diluted to the concentrations needed in 10 mM HEPES/EDTA buffer and then added to the lipid films. The samples were vortexed for approx. 5 s and then left at room temperature overnight, before vortexing again and collecting the samples.

For lipoplexes prepared via the ethanol injection method, the lipids were dissolved in pure ethanol, mixed in the ratios needed, and then injected into a glass vial containing mRNA diluted to the appropriate concentrations with a 10 mM aqueous glycylglycine solution. The injection was done by hand, using 1 mL syringes and 27G needles, under constant stirring from a magnetic stirrer at 500 rpm.

**Sample Composition and Nomenclature.** Preparations used in this article are named systematically, as shown in Figure 1. The preparation method is declared as either "E" (ethanol injection) or "F" (film method). The cationic or ionizable lipid used for the sample

Table 2. List of Samples Used for SAXS Measurements and Their Composition<sup>a</sup>

sample name	N/P	total lipid concentration (mg/mL)	helper lipid	[wt %]		[wt %]		[wt %]		medium
				[mol %]	cationic lipid	[mol %]	mRNA	[mol %]		
F-TMA-1:1	1:1	100	DOPC	90.0	DOTMA	10.0	R18	5.0	H/E	
				88.5		11.5		11.7		
F-DMA-1:0	N/A	100	DOPC	90.0	DODMA	10.0		0.0	H/E	
				87.7		12.3		0.0		
F-DMA-1:1	1:1	100	DOPC	90.0	DODMA	10.0	R18	5.0	H/E	
				87.7		12.3		11.6		
F-DMA-2:1	2:1	100	DOPC	80.0	DODMA	20.0	R18	5.0	H/E	
				75.9		24.1		11.3		
E-DMA-5:1	5:1	10	DOPC	55.9	DODMA	44.1	R159	4.7	GG	
				50.0		50.0		10.0		
E-TAP-5:1	5:1	10	DOPC	54.2	DOTAP	45.8	R159	4.6	GG	
				50.0		50.0		10.0		
E-DAP-5:1	5:1	10	DOPC	54.8	DODAP	45.2	R159	4.6	GG	
				50.0		50.0		10.0		
E-MC-2:1	2:1	10	DOPC	83.1	DLin-MC3-DMA	16.9	R159	4.4	GG	
				80.0		20.0		10.0		
E-MC-5:1	5:1	10	DOPC	55.1	DLin-MC3-DMA	44.9	R159	4.6	GG	
				50.0		50.0		10.0		

<sup>a</sup>Total lipid is the combined lipid concentration (helper lipid and cationic lipid) at which samples were prepared, which was defined as 100 wt %. The N/P ratio is the (approximate) molar ratio of the cationic charge to the anionic charge within the samples in integer numbers. mol % refers to the total lipid molarity within the sample (mol %(helper lipid) + mol %(cationic lipid) = 100%). The preparation medium was either 10 mM HEPES and 0.1 mM EDTA buffer (H/E) or 10 mM glycylglycine solution (GG).

is noted as a two-to-three-letter code (see the figure). The third part of the sample name describes the charge ratio of the cationic lipid to the mRNA in integer numbers (N/P ratio). The sample compositions were calculated as wt % for the film method and mol% for the ethanol injection method. The amount of the helper lipid can be calculated as 100% minus the cationic lipid content (wt % or mol %). Some example compositions and their exact compositions can be seen in Table 2.

**pH Variation.** For pH variation, phosphate buffers proposed by Sørensen, or variations of these with a higher molarity, were used.<sup>34</sup> Aqueous solutions of  $\text{KH}_2\text{PO}_4$  and  $\text{Na}_2\text{HPO}_4$  at 66.7 or 150 mM were mixed at different ratios and adjusted within  $\pm 0.05$  of the required pH via 0.1 M NaOH or HCl. If these pH buffers had to be mixed with sample buffers such as 10 mM glycylglycine or DPBS, the resulting pH of these mixtures was measured as well.

**Small-Angle X-ray Scattering.** SAXS measurements of the samples prepared via the film method were performed at the EMBL P12 BioSAXS beamline, PETRA III, DESY (Hamburg, Germany).<sup>35</sup> Samples and their respective buffers were individually loaded into an in air glass capillary and measured at a sample–detector distance of 3.0 m ( $q$ -range 0.03–5.1  $\text{nm}^{-1}$ ) and a total lipid concentration of 12.5 mg/mL. Measurements were performed at an X-ray wavelength of 0.124 nm (energy 10 keV) and a flux of  $5 \times 10^{12}$  ph/s, with the beam size at the sample position of  $0.15 \times 0.25 \text{ mm}^2$ . Two-dimensional scattering patterns were collected by a Pilatus 2M detector (Dectris, Switzerland) with an exposure time of 0.095 s. For raw data processing, the software SASFLOW and the ATSAS package were used.<sup>35,36</sup> The scattering signal from the buffer and the background was subtracted from the individual sample profiles after proper scaling via the ATSAS software.

SAXS on the samples gained via ethanol injection was performed at the SAXS1 beamline at LNL Campinas, Brazil. Samples were measured in a vacuum capillary at sample–detector distances of 1.0 m ( $q$ -range 0.13–5.0  $\text{nm}^{-1}$ ) and 1.5 m ( $q$ -range 0.08–2.9  $\text{nm}^{-1}$ ) at a concentration of 2 mg/mL total lipid for 100 or 150 s. The X-ray wavelength was 0.155 nm (energy 8 keV), with an energy resolution  $\Delta E/E$  of 0.1. The beam size at the sample position was  $1.5 \text{ mm}^2$ , with a flux density of approx.  $10^{12} \text{ ph}\cdot\text{s}^{-1} \text{ mm}^{-2}$ . The scattering intensities were collected with a Pilatus 300K detector (Dectris, Switzerland), with the raw data being transformed via an in-house developed

software.<sup>37</sup> The scattering signal from the buffer and the background was again subtracted from the individual samples profiles after proper scaling via the ATSAS software.

**Dynamic Light Scattering and  $\zeta$  Potential.** A Zetasizer Nano ZS (Malvern Instruments, Germany) was used for both size measurements via dynamic light scattering (DLS) and  $\zeta$  potential measurements. For size measurements, samples were diluted with 5 mM NaCl or 10 mM glycylglycine buffer, if needed, so that the final measurement concentration was between 0.1 and 1.0 mg/mL total lipid, and then measured at 25 °C. For  $\zeta$  potential measurements, samples were diluted to 0.1 mg/mL total lipid, transferred to DTS 1070 folded capillary cells (Malvern Instruments, Germany), and then measured at 25 °C. No  $\zeta$  potential could be measured in DPBS, due to the high salt concentration.

**Determination of Accessible mRNA.** The amount of freely accessible mRNA after both lipoplex preparation and stimulation of payload release was measured via fluorescence assays. For this, the commercially available Quant-iT RiboGreen RNA Assay (Thermo Fisher) was used.<sup>38</sup> Measurements were performed using a TECAN Infinite F200 plate reader at 465 nm excitation wavelength and 535 nm emission wavelength. For quantification purposes, a calibration curve consisting of the same mRNA in the same medium as used for the samples was measured. Samples were diluted 1:200 (5  $\mu\text{g}/\text{mL}$  total lipid) in a 1:400 dilution of the RiboGreen stock solution in the appropriate medium, which was added to each well. The amount of freely accessible mRNA was calculated as the  $x$ -fold of that of E-TMA-5:1, normalized to the respective total mRNA concentration used during sample preparation.

**Determination of Free mRNA.** Gels containing 1% agarose and 1× Gel-Red staining agent in 1× TBE were prepared. Samples were prepared at 1 mg/mL total lipid and mixed with 40% glycerol at a ratio of 3:1, before adding 5% (vol) bromophenol blue to each sample and loading the samples onto the gel. The electrophoresis was performed at 114 V in 1× TBE buffer for approx. 60 min. mRNA detection was carried out on a Typhoon trio+ (Amersham Biosciences, U.K.) using the green laser (532 nm wavelength). No absolute quantification was used.

**$pK_a$  Fluorescence Assays.** The determination of the apparent formulation  $pK_a$  was done via a previously published assay utilizing 2-( $p$ -toluidino)-6-naphthalene sulfonic acid (TNS).<sup>30</sup> Measurements

were performed in triplicates on black 96-well plates, with each well containing 90  $\mu\text{L}$  of buffer (as described under pH-variation), 10  $\mu\text{L}$  of the sample (0.1 mg/mL total lipid), and 2  $\mu\text{L}$  of TNS in DMSO (300  $\mu\text{M}$ ). Fluorescence was measured using a TECAN infinite 200Pro plate reader at 325 nm excitation and 435 nm emission wavelength as a top measurement.

**Data Treatment.** Data transformation and analysis was performed using Microsoft Excel (Microsoft), QtiPlot 1.0.0 (IONDEV, Romania), and the ATSAS package (EMBL Hamburg, Germany).<sup>36</sup> Peak fitting of SAXS data was performed with both the "PEAK" software included in the ATSAS package and the multi-peak Lorentzian fit functionality in QtiPlot 1.0.0.

All data are given as a function of the momentum transfer, calculated as below

$$q = \frac{4\pi}{\lambda} \sin\left(\frac{2\theta}{2}\right) \quad \begin{array}{l} q: \text{ scattering vector} \\ \lambda: \text{ X - raywavelength} \\ 2\theta: \text{ scattering angle} \end{array} \quad (1)$$

Multi-peak Lorentz fits for peak analysis were performed with QtiPlot, using the built-in function shown as below

$$\text{intensity} = y_0 + \sum_n^{i=1} \left[ \frac{2 \cdot A_i}{\pi} \cdot \frac{w_i}{4 \cdot (x - x_{c,i})^2 + w_i^2} \right]$$

$y_0$ : offset  
 $A$ : peak area  
 $w$ : peak width (FWHM)  
 $x_c$ : peak center

(2)

From the position ( $x_c$ ) of the first-order peaks, the corresponding repeat distance was calculated using the Bragg equation (formula 3).<sup>28,39</sup>

$$d = \frac{n \cdot 2\pi}{q} \quad \begin{array}{l} d: \text{ dspacing} \\ n: \text{ order of the Bragg reflection} \\ q: \text{ scattering vector} \end{array} \quad (3)$$

The peak width  $w$  gives information on the correlation length inside the ordered arrays, where the correlation length scales with the reciprocal width, i.e., with increasing peak width, the correlation length decreases. For the current systems, the correlation length is considered to be driven by its liquid crystalline organization, where positional order is lost as a function of distance. For the translational spatial correlation function, an exponentially decaying cutoff function is applied, where the correlation length  $\xi$  is the distance at which the positional correlation decreased to  $1/e$ .<sup>28</sup>

$$s(r) = \exp\left(\frac{-r}{\xi}\right)$$

$s$ : autocorrelation function of the cut – off function  
 $r$ : distance  
 $\xi$ : distance at which the position correlation decayed to the value of  $1/e$

(4)

For relating this with the peak shape, different options, depending on the models, are possible. Here, for simplicity, the correlation length as a function of the peak width from Lorentz fitting is given as below<sup>28</sup>

$$\xi = \frac{2}{w} \quad \begin{array}{l} \xi: \text{ correlation length} \\ w: \text{ peak width (FWHM)} \end{array} \quad (5)$$

## ■ ASSOCIATED CONTENT

### Supporting Information

The Supporting Information is available free of charge at <https://pubs.acs.org/doi/10.1021/acs.langmuir.0c02446>.

Determination of accessible and free mRNA. RiboGreen accessible mRNA (top) and  $\zeta$  potential (bottom) as a function of the N/P ratio for different formulations (Figure S1); determination of free mRNA via Agarose gels (Figure S2); size reproducibility (Figure S3); relationship between the N/P of systems comprising DODMA and the maximum pH-dependent shift in  $d$  spacing (Figure S4); results of the TNS-based  $pK_a$  assay (Figure S5); Raw peak fitting data from SAXS measurements (Table S1) (PDF)

## ■ AUTHOR INFORMATION

### Corresponding Author

**Peter Langguth** – Department of Pharmaceutics and Biopharmaceutics, Institute of Pharmaceutical and Biomedical Sciences, Johannes Gutenberg University Mainz, D-55099 Mainz, Germany; Phone: 49-6131-3936152; Email: [langguth@uni-mainz.de](mailto:langguth@uni-mainz.de)

### Authors

**Lukas Uebbing** – Department of Pharmaceutics and Biopharmaceutics, Institute of Pharmaceutical and Biomedical Sciences, Johannes Gutenberg University Mainz, D-55099 Mainz, Germany; [orcid.org/0000-0003-0568-9540](https://orcid.org/0000-0003-0568-9540)

**Antje Ziller** – Department of Pharmaceutics and Biopharmaceutics, Institute of Pharmaceutical and Biomedical Sciences, Johannes Gutenberg University Mainz, D-55099 Mainz, Germany

**Christian Siewert** – Department of Pharmaceutics and Biopharmaceutics, Institute of Pharmaceutical and Biomedical Sciences, Johannes Gutenberg University Mainz, D-55099 Mainz, Germany

**Martin A. Schroer** – European Molecular Biology Laboratory (EMBL) Hamburg Outstation c/o DESY, 22607 Hamburg, Germany; [orcid.org/0000-0002-0747-3965](https://orcid.org/0000-0002-0747-3965)

**Clement E. Blanchet** – European Molecular Biology Laboratory (EMBL) Hamburg Outstation c/o DESY, 22607 Hamburg, Germany

**Dmitri I. Svergun** – European Molecular Biology Laboratory (EMBL) Hamburg Outstation c/o DESY, 22607 Hamburg, Germany

**Srinivas Ramishetti** – Laboratory of Precision NanoMedicine, Shmunis School for Biomedicine and Cancer Research, George S. Wise Faculty of Life Sciences, Tel Aviv University, Tel Aviv 69978, Israel

**Dan Peer** – Laboratory of Precision NanoMedicine, Shmunis School for Biomedicine and Cancer Research, George S. Wise Faculty of Life Sciences, Tel Aviv University, Tel Aviv 69978, Israel; [orcid.org/0000-0001-8238-0673](https://orcid.org/0000-0001-8238-0673)

**Ugur Sahin** – BioNTech RNA Pharmaceuticals GmbH, 55131 Mainz, Germany; TRON - Translational Oncology at the University Medical Center of Johannes Gutenberg University Mainz gGmbH, 55099 Mainz, Germany; Research Center for Immunotherapy (FZI), University Medical Center at the Johannes Gutenberg University Mainz, 55099 Mainz, Germany

**Heinrich Haas** – BioNTech RNA Pharmaceuticals GmbH, 55131 Mainz, Germany; [orcid.org/0000-0002-5517-5970](https://orcid.org/0000-0002-5517-5970)

Complete contact information is available at:

<https://pubs.acs.org/10.1021/acs.langmuir.0c02446>

## Funding

This research was funded by the “Deutsche Forschungsgemeinschaft DFG” as part of the collaborative research center (CRC) 1066. The DFG had no involvement in study design, collection, analysis, interpretation of data, writing of the report, and in the decision to submit the article for publication. DLin-MC3-DMA was a gift from the Dan Peer Group (Tel Aviv University, Israel).

## Notes

The authors declare no competing financial interest.

## ACKNOWLEDGMENTS

Funding by the “Deutsche Forschungsgemeinschaft” (SFB 1066) is gratefully acknowledged. P. Langguth is an advisor to BioNTech. This research used resources of the Brazilian Synchrotron Light Laboratory (LNLS), an open national facility operated by the Brazilian Centre for Research in Energy and Materials (CNPEM) for the Brazilian Ministry for Science, Technology, Innovations and Communications (MCTIC). The SAXS1 beamline staff, as represented by Carla Pólo and Tiago Kalile, is acknowledged for the assistance during the experiments. We would like to thank Cristina Sala for the preparation of the graphical abstract.

## ABBREVIATIONS

mRNA, messenger ribonucleic acid; DOTMA, 1,2-di-*O*-octadecenyl-3-trimethylammonium propane; DOTAP, 1,2-dioleoyl-3-trimethylammonium-propane; DOPC, 1,2-dioleoyl-*sn*-glycero-3-phosphocholine; DOPE, 1,2-dioleoyl-*sn*-glycero-3-phosphoethanolamine; DLin-DMA, 1,2-dilinoleoxy-3-dimethylaminopropane; DLin-KC2-DMA, 2,2-dilinoleyl-4-dimethylaminoethyl-[1,3]-dioxolane; DLin-MC3-DMA, [(6Z,9Z,28Z,31Z)-heptatriaconta-6,9,28,31-tetraen-19-yl] 4-(dimethylamino)butanoate; DNA, desoxyribonucleic acid; siRNA, small interfering ribonucleic acid; SAXS, small-angle X-ray scattering; DODAP, 1,2-dioleoyl-3-dimethylammonium-propane; DODMA, 1,2-dioleoyl-3-dimethylaminopropane; EDTA, ethylenediaminetetraacetic acid; HEPES, 4-(2-hydroxyethyl)-1-piperazineethanesulfonic acid; DPBS, Dulbecco's phosphate-buffered saline; DMSO, dimethyl sulfoxide; TNS, 6-(*p*-toluidino)-2-naphthalenesulfonic acid sodium salt; DLS, dynamic light scattering; LNP, lipid nanoparticle

## REFERENCES

- (1) Sahin, U.; Kariko, K.; Tureci, O. mRNA-based therapeutics—developing a new class of drugs. *Nat. Rev. Drug Discovery* **2014**, *13*, 759–780.
- (2) Yamamoto, A.; Kormann, M.; Rosenecker, J.; Rudolph, C. Current prospects for mRNA gene delivery. *Eur. J. Pharm. Biopharm.* **2009**, *71*, 484–489.
- (3) Ziller, A.; Nogueira, S. S.; Huehn, E.; Funari, S. S.; Brezesinski, G.; Hartmann, H.; Sahin, U.; Haas, H.; Langguth, P. Incorporation of mRNA in lamellar lipid matrices for parenteral administration. *Mol. Pharmaceutics* **2018**, *15*, 642–651.
- (4) Kranz, L. M.; Diken, M.; Haas, H.; Kreiter, S.; Loquai, C.; Reuter, K. C.; Meng, M.; Fritz, D.; Vascotto, F.; Hefesha, H.; et al. Systemic RNA delivery to dendritic cells exploits antiviral defence for cancer immunotherapy. *Nature* **2016**, *534*, 396–401.
- (5) Grabbe, S.; Haas, H.; Diken, M.; Kranz, L. M.; Langguth, P.; Sahin, U. Translating nanoparticulate-personalized cancer vaccines into clinical applications: case study with RNA-lipoplexes for the treatment of melanoma. *Nanomedicine* **2016**, *11*, 2723–2734.

- (6) Sahin, U.; Derhovanessian, E.; Miller, M.; Kloke, B.-P.; Simon, P.; Löwer, M.; Bukur, V.; Tadmor, A. D.; Luxemburger, U.; Schrörs, B.; et al. Personalized RNA mutanome vaccines mobilize poly-specific therapeutic immunity against cancer. *Nature* **2017**, *547*, 222–226.

- (7) Rosigkeit, S.; Meng, M.; Grunwitz, C.; Gomes, P.; Kreft, A.; Hayduk, N.; Heck, R.; Pickert, G.; Ziegler, K.; Abassi, Y.; et al. Monitoring Translation Activity of mRNA-Loaded Nanoparticles in Mice. *Mol. Pharmaceutics* **2018**, *15*, 3909–3919.

- (8) Siewert, C.; Haas, H.; Nawroth, T.; Ziller, A.; Nogueira, S. S.; Schroer, M. A.; Blanchet, C. E.; Svergun, D. I.; Radulescu, A.; Bates, F.; et al. Investigation of charge ratio variation in mRNA - DEAE-dextran polyplex delivery systems. *Biomaterials* **2019**, *192*, 612–620.

- (9) Sahin, U.; Türeci, Ö. Personalized vaccines for cancer immunotherapy. *Science* **2018**, *359*, 1355–1360.

- (10) Kreiter, S.; Diken, M.; Selmi, A.; Türeci, Ö.; Sahin, U. Tumor vaccination using messenger RNA: prospects of a future therapy. *Curr. Opin. Immunol.* **2011**, *23*, 399–406.

- (11) Pastor, F.; Berraondo, P.; Etxeberria, I.; Frederick, J.; Sahin, U.; Gilboa, E.; Melero, I. An RNA toolbox for cancer immunotherapy. *Nat. Rev. Drug Discovery* **2018**, *17*, 751–767.

- (12) Elouahabi, A.; Ruyschaert, J.-M. Formation and intracellular trafficking of lipoplexes and polyplexes. *Mol. Ther.* **2005**, *11*, 336–347.

- (13) Marchini, C.; Pozzi, D.; Montani, M.; Alfonsi, C.; Amici, A.; Amenitsch, H.; Candeloro De Sanctis, S.; Caracciolo, G. Tailoring lipoplex composition to the lipid composition of plasma membrane: a Trojan horse for cell entry? *Langmuir* **2010**, *26*, 13867–13873.

- (14) Felgner, J. H.; Kumar, R.; Sridhar, C. N.; Wheeler, C. J.; Tsai, Y. J.; Border, R.; Ramsey, P.; Martin, M.; Felgner, P. L. Enhanced gene delivery and mechanism studies with a novel series of cationic lipid formulations. *J. Biol. Chem.* **1994**, *269*, 2550–2561.

- (15) Rietwyk, S.; Peer, D. Next-Generation Lipids in RNA Interference Therapeutics. *ACS Nano* **2017**, *11*, 7572–7586.

- (16) Kedmi, R.; Ben-Arie, N.; Peer, D. The systemic toxicity of positively charged lipid nanoparticles and the role of Toll-like receptor 4 in immune activation. *Biomaterials* **2010**, *31*, 6867–6875.

- (17) Torchilin, V. P.; Zhou, F.; Huang, L. pH-Sensitive Liposomes. *J. Liposome Res.* **1993**, *3*, 201–255.

- (18) Ramezani, M.; Schmidt, M. L.; Bodnariuc, I.; Kulkarni, J. A.; Leung, S. S. W.; Cullis, P. R.; Thewalt, J. L.; Tieleman, D. P. Ionizable amino lipid interactions with POPC: implications for lipid nanoparticle function. *Nanoscale* **2019**, *11*, 14141.

- (19) Kauffman, K. J.; Dorkin, J. R.; Yang, J. H.; Heartlein, M. W.; DeRosa, F.; Mir, F. F.; Fenton, O. S.; Anderson, D. G. Optimization of Lipid Nanoparticle Formulations for mRNA Delivery in Vivo with Fractional Factorial and Definitive Screening Designs. *Nano Lett.* **2015**, *15*, 7300–7306.

- (20) Semple, S. C.; Akinc, A.; Chen, J.; Sandhu, A. P.; Mui, B. L.; Cho, C. K.; Sah, D. W. Y.; Stebbing, D.; Crosley, E. J.; Yaworski, E.; et al. Rational design of cationic lipids for siRNA delivery. *Nat. Biotechnol.* **2010**, *28*, 172–176.

- (21) Jayaraman, M.; Ansell, S. M.; Mui, B. L.; Tam, Y. K.; Chen, J.; Du, X.; Butler, D.; Eltepu, L.; Matsuda, S.; Narayanannair, J. K.; et al. Maximizing the potency of siRNA lipid nanoparticles for hepatic gene silencing in vivo. *Angew. Chem., Int. Ed.* **2012**, *51*, 8529–8533.

- (22) Olden, B. R.; Cheng, E.; Cheng, Y.; Pun, S. H. Identifying key barriers in cationic polymer gene delivery to human T cells. *Biomater. Sci.* **2019**, *7*, 789–797.

- (23) Nogueira, S.; Schlegel, A.; Maxeiner, K.; Weber, B.; Barz, M.; Schroer, M. A.; Blanchet, C. E.; Svergun, D.; Ramishetti, S.; Peer, D.; Langguth, P.; Sahin, U.; Haas, H. Polysarcosine-Functionalized Lipid Nanoparticles for Therapeutic mRNA Delivery. *ACS Appl. Nano Mater.* **2020**, DOI: 10.1021/acsnano.0c01834.

- (24) Akinc, A.; Maier, M. A.; Manoharan, M.; Fitzgerald, K.; Jayaraman, M.; Barros, S.; Ansell, S.; Du, X.; Hope, M. J.; Madden, T. D.; et al. The Onpatro story and the clinical translation of nanomedicines containing nucleic acid-based drugs. *Nat. Nanotechnol.* **2019**, *14*, 1084–1087.

(25) Seddon, J. M.; Templer, R. H. Polymorphism of Lipid-Water Systems. *Structure and Dynamics of Membranes—From Cells to Vesicles; Handbook of Biological Physics*; Elsevier, 1995; pp 97–160.

(26) Nagle, J. F.; Tristram-Nagle, S. Structure of lipid bilayers. *Biochim. Biophys. Acta, Rev. Bioembr.* **2000**, *1469*, 159–195.

(27) Tristram-Nagle, S.; Petrache, H. I.; Nagle, J. F. Structure and Interactions of Fully Hydrated Dioleoylphosphatidylcholine Bilayers. *Biophys. J.* **1998**, *75*, 917–925.

(28) Agra-Kooijman, D. M.; Kumar, S. X-ray Scattering Investigations of Liquid Crystals. In *Handbook of Liquid Crystals*; Goodby, J. W.; Tschierske, C.; Raynes, P.; Gleeson, H.; Kato, T.; Collings, P. J., Eds.; Wiley-VCH Verlag GmbH & Co. KGaA: Weinheim, Germany, 2014; pp 1–38.

(29) Cullis, P. R.; Hope, M. J. Lipid Nanoparticle Systems for Enabling Gene Therapies. *Mol. Ther.* **2017**, *25*, 1467–1475.

(30) Heyes, J.; Palmer, L.; Bremner, K.; MacLachlan, I. Cationic lipid saturation influences intracellular delivery of encapsulated nucleic acids. *J. Controlled Release* **2005**, *107*, 276–287.

(31) Litzinger, D. C.; Huang, L. Phosphatidylethanolamine liposomes: drug delivery, gene transfer and immunodiagnostic applications. *Biochim. Biophys. Acta, Rev. Biomembr.* **1992**, *1113*, 201–227.

(32) Siewert, C. D.; Haas, H.; Cornet, V.; Nogueira, S. S.; Nawroth, T.; Uebbing, L.; Ziller, A.; Al-Gousous, J.; Radulescu, A.; Schroer, M. A.; Blanchet, C. E.; Svergun, D. I.; Radsak, M. P.; Sahin, U.; Langguth, P. Hybrid Biopolymer and Lipid Nanoparticles with Improved Transfection Efficacy for mRNA. *Cells* **2020**, *9*, No. 2034.

(33) Kuhn, A. N.; Diken, M.; Kreiter, S.; Selmi, A.; Kowalska, J.; Jemielity, J.; Darzynkiewicz, E.; Huber, C.; Türeci, O.; Sahin, U. Phosphorothioate cap analogs increase stability and translational efficiency of RNA vaccines in immature dendritic cells and induce superior immune responses in vivo. *Gene Ther.* **2010**, *17*, 961–971.

(34) Romeis, B. *Mikroskopische Technik*, 16th ed.; R. Oldenbourg Verlag: München, 1968.

(35) Blanchet, C. E.; Spilotros, A.; Schwemmer, F.; Graewert, M. A.; Kikhney, A.; Jeffries, C. M.; Franke, D.; Mark, D.; Zengerle, R.; Cipriani, F.; et al. Versatile sample environments and automation for biological solution X-ray scattering experiments at the P12 beamline (PETRA III, DESY). *J. Appl. Crystallogr.* **2015**, *48*, 431–443.

(36) Franke, D.; Petoukhov, M. V.; Konarev, P. V.; Panjkovich, A.; Tuukkanen, A.; Mertens, H. D. T.; Kikhney, A. G.; Hajizadeh, N. R.; Franklin, J. M.; Jeffries, C. M.; et al. ATSAS 2.8: a comprehensive data analysis suite for small-angle scattering from macromolecular solutions. *J. Appl. Crystallogr.* **2017**, *50*, 1212–1225.

(37) SAXS1—LNLS: Overview, 2019. <https://www.lnls.cnpem.br/linhas-de-luz/saxs1-en/overview/> (accessed March 8, 2019).

(38) Molecular Probes, I. Quant-iT RiboGreen RNA Reagent and Kit: MP 11490. <https://www.thermofisher.com/document-connect/document-connect.html?url=https%3A%2F%2Fassets.thermofisher.com%2F2FTFS-Assets%2F2FLSG%2Fmanuals%2Fmp11490.pdf&title=UXVhbnQtaVQgUmlib0dyZWVuIFJlOQBSZWFnZW50IGFuZCBLaXQ=>.

(39) Bragg, W. H.; Bragg, W. L. The reflection of X-rays by crystals. *Proc. R. Soc. London, Ser. A* **1913**, *88*, 428–438.